

VLA DETECTION OF RRLS FROM THE RADIO NUCLEUS OF NGC 253 :
IONIZATION BY A WEAK AGN, AN OBSCURED SSC OR A COMPACT SNR ?

NIRUJ R. MOHAN

Raman Research Institute, C.V. Raman Avenue, Sadashivanagar Post Office, Bangalore 560080, India

and

Joint Astronomy Program, Department of Physics, Indian Institute of Science, Bangalore 560012, India

niruj@rri.res.in

AND

K.R. ANANTHARAMAIAH ¹

Raman Research Institute, C.V. Raman Avenue, Sadashivanagar Post Office, Bangalore 560080, India

AND

W.M. GOSS

National Radio Astronomy Observatory, PO Box O, Socorro, NM 87801, USA

mgoss@aoc.nrao.edu

Draft version October 28, 2018

ABSTRACT

We have imaged the H92 α and H75 α radio recombination line (RRL) emissions from the starburst galaxy NGC 253 with a resolution of ~ 4 pc. The peak of the RRL emission at both frequencies coincides with the unresolved radio nucleus. Both lines observed towards the nucleus are extremely wide, with FWHM of ~ 200 km s⁻¹. Modeling the RRL and radio continuum data for the radio nucleus shows that the lines arise in gas whose density is $\sim 10^4$ cm⁻³ and mass is few thousand M_{\odot} , which requires an ionizing flux of 6–20 $\times 10^{51}$ photons s⁻¹. We consider a SNR expanding in a dense medium, a star cluster and also an AGN as potential ionizing sources. Based on dynamical arguments, we rule out an SNR as a viable ionizing source. A star cluster model was considered and the dynamics of the ionized gas in a stellar-wind driven structure was investigated. Such a model is consistent with the properties of the ionized gas only for a cluster younger than $\sim 10^5$ years. The existence of such a young cluster at the nucleus seems improbable. The third model assumes the ionizing source to be an AGN at the nucleus. In this model, it was shown that the observed X-ray flux is too weak to account for the required ionizing photon flux. However, the ionization requirement can be explained if the accretion disk is assumed to have a Big Blue Bump in its spectrum. Hence, we favor an AGN at the nucleus as the source responsible for ionizing the observed RRLs. A hybrid model consisting of an inner ADAF disk and an outer thin disk is suggested, which could explain the radio, UV and the X-ray luminosities of the nucleus.

Subject headings: galaxies: individual (NGC 253) — galaxies: ISM — galaxies: nuclei — galaxies: starburst — radio lines: galaxies

1. INTRODUCTION

NGC 253 is a nearby (D=2.5 Mpc) spiral galaxy with the central ~ 100 pc hosting a vigorous starburst. The ionized gas in this region, studied by its emission in the radio, infra-red and the optical, consists of both compact and diffuse components and is distributed along a highly inclined ring. Turner and Ho (1985) discovered a string of compact sources at 15 GHz, which were studied in detail by Antonucci and Ulvestad (1988) and Ulvestad and Antonucci (1997). A number of infra-red (IR) hotspots have also been imaged in this region (Forbes, Ward, and Depoy 1991; Forbes et al. 1993; Piña et al. 1992; Keto et al. 1993; Sams et al. 1994). Kalas and Wynn-Williams (1994) and Sams et al (1994) showed that most of these hotspots are regions of low dust extinction and are not coincident with the radio sources. Optical imaging by Watson et al. (1996) revealed the presence of four star clusters, which were identified with individual IR knots (see also Forbes

et al. 2000). The radio and the IR-optical sources seem to trace different populations of objects, presumably supernova remnants and HII regions, respectively. Radio recombination lines (RRLs) have been observed from this galaxy in the cm (Seaquist and Bell 1977; Mebold et al. 1980; Anantharamaiah and Goss 1996) and mm (Puxley et al. 1997) wavebands with a resolution of a few arcseconds ($1''=12$ pc) or larger. Since IR and radio continuum images are now available with sub-arcsecond resolution, the identification of the exact sources of RRL emission using high resolution imaging becomes relevant.

The peak of the IR emission is offset by about $3.5''$ southwest from the peak of the radio continuum emission (the radio nucleus). There is no associated radio emission towards the IR peak and weak IR emission is observed near the radio nucleus. Keto et al. (1999) have shown that the IR peak hosts a super star cluster (SSC) and they have also suggested that the radio nucleus is probably an AGN. Turner & Ho (1985), based on their high-

¹ Deceased Oct. 29, 2001.

resolution VLA image of the 15 GHz continuum emission, discovered that the radio nucleus is an unresolved source with high brightness temperature and suggested that the nucleus could harbor an AGN. Multi-band tracers of ionized gas ([NeII]: Böker, Krabbe and Storey 1998; Keto et al. 1999; Br γ : Forbes et al. 1993; optical continuum and line emission: Engelbracht et al. 1998; Watson et al. 1996; Forbes et al. 2000) show that the maximum emission at these wavebands coincide with the position of the IR peak. It is therefore surprising that the cm-wave RRL emission imaged by Anantharamaiah and Goss (1996) with a resolution of $1.8'' \times 1''$ shows that the recombination line emission peaks at the radio nucleus, with much weaker emission near the IR peak. In order to further investigate the characteristics of this emission, we have carried out sub-arcsecond observations of the RRL emission from NGC 253 at 8.3 and 15 GHz using the VLA. These observations will help identify the compact continuum sources from which the RRLs observed at low resolutions originate. Additionally, since the peak of the line emission is probably coincident with the radio nucleus, the physical properties of the ionized gas in this region, and hence the nature of the nuclear source can be derived by modeling the RRL emission.

2. OBSERVATIONS AND RESULTS

The 8.3 GHz H92 α and the 15 GHz H75 α recombination lines from NGC 253 were observed using the Very Large Array of the National Radio Astronomy Observatory in the A configuration. This observing mode yields the required parsec-scale resolution with the best sensitivity possible. The data analysis was done using standard procedures available in the software package AIPS. The datasets at 8.3 GHz, acquired over three periods, were concatenated for further processing. Of the two datasets available at 15 GHz, only one was used as the other suffered from bandpass problems. Continuum images were made at both frequencies and are consistent with the images published by Ulvestad and Antonucci (1997). The channel visibilities, after hanning smoothing off-line to reduce the effects of Gibbs ringing, were used to construct line datacubes. The continuum and line images at both frequencies were convolved to a common resolution of $0.35'' \times 0.22''$ at a P.A. of -10° . The shortest baselines in the datasets are mentioned in Table 1. The largest well-sampled angular scale in the images are estimated to be $\sim 7.5''$ at 8.3 GHz and $\sim 3.0''$ at 15 GHz.

The continuum emission at 8.3 GHz and 15 GHz from the central $3''$ region are shown in Figure 1. Also shown in the figure are overlays of the integrated line emission. The H92 α and H75 α spectra towards the peak of the line emission are shown in Figure 2. Further observational details and image parameters are listed in Table 1. The peak of the continuum emission corresponds to the radio nucleus and is associated with the source 5.79-39.0 in the compact source catalog of Ulvestad and Antonucci (1997). Though the central $3''$ region contains multiple sources, the nucleus is separable from the surrounding emission with our resolution of $0.3''$. The peaks of both the H92 α and H75 α line emission coincide with the unresolved radio nucleus, with much weaker emission near the IR peak. Extended H92 α line emission is detected over a $3''$ region. Since the

8.3 GHz datasets were imaged with less weighting given to short spacing visibilities in order to have similar resolution as that of the 15 GHz data, this diffuse emission is not detectable in Figure 1. In this paper, we will only discuss the line emission detected against the unresolved radio nucleus. The discussion of the extended line emission as well as the emission towards other compact sources in the field will follow in a later paper.

3. MODELING THE RRL EMISSION

The properties of the ionized gas at the nucleus were modeled using the observed continuum and recombination lines. These observational constraints correspond to an area of ~ 4 pc (one synthesized beam) and the values are listed in Table 1. The line emitting gas was assumed to be photo-ionized and the atomic level populations were derived assuming that the gas is not in local thermodynamic equilibrium (non-LTE). The ionized gas was modeled as a single spherical HII region, a collection of HII regions and also as a rectangular slab. Since the results are similar in all three cases, we will only discuss the spherical HII region model. The free parameters of the model are electron density (n_e), diameter (l) of the HII region and electron temperature (T_e); the range of parameter space is indicated in Table 2. The density was assumed to be uniform inside the HII region. The relative locations of both the line emitting thermal gas and the non-thermal continuum source along the line of sight within the synthesized beam are unknown. Hence, the fraction of the non-thermal continuum radiation which is behind the thermal gas (and is responsible for stimulated line emission due to background radiation) is varied from zero to the total observed flux density in the models. For every combination of n_e , l and T_e , the continuum and line emission strengths were then calculated. Of these combinations, those models which reproduce the observed line strengths at both frequencies and also predict continuum flux densities consistent with the observed values were accepted as valid solutions. The spectral index of the unabsorbed continuum (which includes the non-thermal part as well the thermal part which does not contribute to the observed line emission) was also calculated and was constrained not to be steeper than -1.0 . The details of the modeling technique are discussed in detail by Anantharamaiah et al. (1993).

The range of values for various solutions are indicated in Table 2. The results do not depend sensitively on the assumed value of the electron temperature within the range explored. Typical parameters of the line emitting gas are listed in Table 3 for specific models. The allowed models described in Tables 1 and 2 assume that the unabsorbed continuum fills the synthesized beam. No solutions were obtained if the gas is assumed to be in LTE; the linear size of the region is too small and the background non-thermal radiation is too weak to produce a detectable RRL. Hence line enhancement due to non-LTE processes is essential to explain the observed line strength. Only a narrow range of densities ($6 \times 10^3 - 1.7 \times 10^4 \text{ cm}^{-3}$) is allowed and the ionizing photon rate ranges from $6 - 20 \times 10^{51}$ photons s^{-1} . A power-law multi-density model was also considered (see Model IV of Mohan et al. 2001 for details). In this model, gas at densities which differ considerably from the values derived in this section will not

contribute appreciably to the observed RRL emission (see Mohan et al. 2001). Hence the constant density approximation used in the models mentioned above is justified. For $n_e < 6 \times 10^3 \text{ cm}^{-3}$, the computed line emissions inside a ~ 4 pc region falls short of the observed values. For $n_e > 1.7 \times 10^4 \text{ cm}^{-3}$, the model predictions do not agree with the observed H92 α /H75 α line ratio. The observations can be explained without invoking stimulated emission due to a background continuum radiation, i.e., the line emission can be explained solely by spontaneous emission by ionized gas, which includes stimulated emission by its own thermal continuum. For a given emission measure, inclusion of any externally stimulated emission enhances the recombination line strength compared with a case where no background radiation is invoked. Hence, the mass of ionized gas needed and the required ionizing photon flux are both less by up to a factor 2–3 for models incorporating non-thermal continuum radiation. If the unabsorbed continuum is assumed to be a distributed uniform background, then the externally stimulated emission can account for up to 60–70 % of the total H75 α line strength.

If these models are computed for either the H92 α or the H75 α line alone, the range of allowed densities obtained is larger. Including only the H92 α line changes the lower limit to the allowed density to 2000 cm^{-3} , whereas, densities as high as 10^5 cm^{-3} are allowed for models which incorporate only the H75 α line. Thus, including both RRLs constrains the possible density to a much narrower range, assuming that all of the observed line emission at both frequencies arises in the same region of ionized gas. Our models, therefore, show that the observed H75 α and H92 α lines arise in gas with a mass of a few thousand M_\odot , a density of $\sim 10^4 \text{ cm}^{-3}$ and require an ionizing photon flux of $\geq 6 \times 10^{51} \text{ s}^{-1}$. The relative faintness of RRLs from near the IR peak, and the absence of a strong radio counterpart to the IR peak, which is a massive SSC, does not necessarily imply that there is less gas at the latter position; the gas could be of lower density instead.

4. THE IONIZING SOURCE

The RRL detection from the unresolved radio nucleus is from a sufficiently small linear size that the interpretation is not complicated by the unknown beam filling factors of the gas. The derived ionizing photon flux inside a $\sim 0.3''$ (4 pc) region can be compared with the values computed from other tracers of ionized gas. Using photo-ionization models, this value corresponds to a H α flux of $1.2 \times 10^{-14} \text{ W/m}^2$. Forbes et al (2000) list the H α fluxes of compact optical sources measured inside a $0.4''$ aperture. Since the strength of the line emission at the position of the radio nucleus is weak (Watson et al. 1996 and Forbes, private communication), we can assume that the H α flux from this area is less than that of the weakest source listed in their table. Then the extinction derived using the H α estimated from RRL modeling is $A_V > 14^m$, consistent with the $A_V = 24^m \pm 6$ derived by Sams et al. (1994) towards the radio nucleus. Measurements of other IR emission lines from ionized gas correspond to much larger apertures and since the region surrounding the radio nucleus does contain significant amounts of ionized gas, a direct comparison is difficult. Nevertheless, if we assume an uniform extinction of 25^m in the central region, then the extinction corrected

Br α flux from the central $6''$ (from the data of Beck & Beckwith 1984) is a factor of 10 higher than the predictions of our model for the $\sim 0.3''$ region of the nucleus. Forbes et al. (1993) measured the Br γ emission inside a $2''$ aperture centered around the radio nucleus (referred to as spot A). The Br γ flux measured by them is a factor of two higher than the value predicted by our models, this excess being possibly due to their larger aperture.

Since the region of interest is highly obscured, the source of the photo-ionization remains uncertain. We have considered three possible candidates : (1) supernova remnant expanding in a dense medium, (2) stellar cluster and (3) AGN. Each of these will now be examined in detail to investigate which of these can explain the observed properties of the nuclear region. The imposed constraints are the derived properties of the ionized gas like density, size, ionizing flux and line width and also the radio, UV (derived from ionization) and X-ray luminosities of the nucleus. The 2–10 keV X-ray luminosity (L_{2-10}) of the X-ray source coincident with the radio nucleus is $7 \times 10^{38} \text{ ergs s}^{-1}$ (unresolved for $E > 2 \text{ keV}$; Pietsch et al. 2001, using the *XMM-NEWTON*).

5. A COMPACT SUPERNOVA REMNANT AS AN IONIZING SOURCE

Chevalier and Fransson (2001) invoked a supernova remnant (SNR) expanding into a dense ambient medium to explain some of the compact radio sources in the starburst galaxy M 82 and in Arp 220 as well and we now consider such a model to explain the nucleus of NGC 253. The high ambient density slows down the expansion to a few 100 km s^{-1} , confines the remnant to a smaller size, and causes it to quickly enter the radiative or snowplow phase. These factors could explain the spatial extent (≤ 4 pc) and the line width (attributed to the expansion of the remnant) of the ionized gas. In the snowplow phase, the swept-up gas cools and forms a thin shell, and can be ionized by the X-ray photons from the hot gas inside the remnant, giving rise to the observed RRLs. We have calculated the dynamics and radiation of such an SNR in an attempt to explain the RRL observations. In our model, the input parameters are the initial energy of the explosion, E_o , the ambient density, n_o , and the age of the compact SNR. Following the work of Draine and Woods (1991), we calculate the velocity and radius of the shock front and also the ionization rate and the density of ionized gas in the shell as a function of time, E_o and n_o . The time dependent value of L_{2-10} was also computed for both the Sedov phase (using the similarity solutions; Newman 1977) and for the radiative phase. The observed values (listed in Table 1 and 2) are compared with these calculated values for the radiative phase of the SNR (when an expanding recombining gas is produced). We find that the models cannot simultaneously satisfy all of these constraints for any combination of input parameters. Hence the properties of the nucleus cannot be explained by an SNR expanding in a dense medium.

6. A STAR CLUSTER AS AN IONIZING SOURCE

In this section, we assume that the nucleus hosts a stellar cluster and derive its properties. The number of O stars necessary to produce $> 6 \times 10^{51} \text{ photons s}^{-1}$ is > 450 and

the total mass of the cluster is $> 8.5 \times 10^4 M_{\odot}$ (computed assuming a Salpeter IMF with a mass range between 1–80 M_{\odot} and using the tables in Vacca, Garmany and Shull 1996). Since the region modeled is ~ 4 pc in extent, the resultant total stellar mass and the lower limit to the stellar surface density imply that the ionizing source must be a super star cluster (SSC; Meurer et al 1995). The RRLs are assumed to arise in the HII region around this SSC (similar to ‘supernebulae’ discovered in centers of other galaxies: Kobulnicky and Johnson 1999; Neff and Ulvestad 2000; Tarchi et al. 2000; Turner, Beck and Ho 2000; Mohan et al. 2001). The detection of wide lines with FWHM of $\sim 200 \text{ km s}^{-1}$ from within a ~ 4 pc region is a constraint on the dynamics of the nebula, which we investigate below. It should be noted that the dynamical age of the gas (\sim radius/velocity) is $\sim 10^4$ years and the sound crossing time is $\sim 10^5$ years.

6.1. Gas dynamics of the ‘supernebula’

Though a HII region ionized by a central cluster will expand outwards, its expansion velocity can never exceed the speed of sound in the ionized medium (Spitzer 1968) and hence cannot account for the wide lines observed. Also champagne flows in HII regions cannot produce velocities larger than $\sim 50 \text{ km s}^{-1}$ (Yorke, Tenorio-Tagle and Bodenheimer 1984). Though supersonic velocities are known in extragalactic HII regions, their line widths are only ~ 30 – 100 km s^{-1} and the HII regions are also much larger in size (for eg., Muñoz-Tuñón, Tenorio-Tagle and Casteñada 1996). The only plausible way to explain the observed velocity width is by invoking a stellar-wind driven HII region expanding at $\sim 100 \text{ km s}^{-1}$. The expansion velocity of a wind-driven shell scales as $(L_{\text{mech}})^{1/5}$, where L_{mech} is the mechanical luminosity of the wind and hence a expansion velocity of 100 km s^{-1} for a cluster whose L_{mech} is $\sim 10^3$ times that of an O star is easily obtainable. The dynamical age of a wind-driven shell is $\sim 0.55 \times R_{\text{shell}}/V_{\text{shell}}$ (McCray 1983), i.e., $\sim 10^4$ years.

The model considered here is that of a uniform density nebula whose dynamics is determined by the ionizing photons and the stellar wind of a central SSC. In the wind-driven phase of expansion, the nebula quickly enters the snowplow phase ($\leq 10^3$ years), wherein it can be either in the energy-conserving or in the momentum-conserving phase. The swept-up matter forms a thin shell which is assumed to trap all the ionizing photons. The input parameters are the star formation history of the cluster, the constant ambient density (n_0) and the age of the cluster (assumed to be the same as the nebula) and the range of parameter space explored is summarized in Table 4. The time dependent values of $N_{\text{Ly}\alpha}$ and L_{mech} were derived from simulations using the code Starburst 99² (Leitherer et al. 1999). This simulation was carried out for solar metallicity and a Salpeter initial mass function with an upper mass cut-off of $100 M_{\odot}$. These values were obtained both for a continuous and an instantaneous star formation history for a particular value of star formation rate (SFR) and subsequently scaled linearly for other values of SFR. For a given combination of input parameters, the radius and velocity of the shock front (almost the same as that of the ionized gas), mass of ionized gas, ionization rate and

the gas density were computed. These calculations were carried out using the expressions in Shull (1980) for the appropriate phase of the nebula. The derived values were compared with the values derived from the RRL modeling, listed in Table 4. Acceptable solutions were identified which were consistent with the imposed constraints. Table 4 summarizes the allowed parameters.

Gas dynamics narrowly constrains the properties of the possible supernebula. The derived solutions correspond to wind-driven shells in the energy-conserving phase. The allowed age of the nebula (and hence the cluster) is $\sim 2.5 \times 10^4$ years, corresponding to a diameter of 7–8 pc; no solutions for smaller sizes were found. These values are a strong constraint on the hypothesized SSC. However, the reliability of these values depends on the accuracy of the Starburst 99 code for young clusters, as discussed in section 8.1.

7. A WEAK AGN AS AN IONIZING SOURCE

Turner & Ho (1985) discovered that the nucleus is unresolved in the radio continuum, and has a high brightness temperature and hence suggested a possible AGN at the nucleus. Ulvestad & Antonucci (1997) also arrived at the same conclusion based on their higher-resolution images. The derived size is $< 0.05''$ and the lower limit to the brightness temperature is between 22 000–90 000 K. If an AGN does exist at the nucleus, then its UV continuum can be invoked to ionize the RRL emitting gas. The expected UV luminosity can be estimated using the observed radio continuum and X-ray luminosities. Based on the upper limit to the size of the ionized gas and the observed line width, the dynamical mass at the center ($\sim \sigma^2 r/G$) is constrained to be less than $3 \times 10^6 M_{\odot}$.

Powerful AGNs are powered by a geometrically thin standard accretion disk whose blackbody emission peaks in the UV, called the Big Blue Bump, or BBB (Koratkar and Blaes 1999), which can provide the required ionization. Falcke et al. (1995) showed that this BBB luminosity is correlated with the core radio emission (νL_{ν} at 2 cm) for a sample of quasars. Extrapolating their relation for radio-weak quasars for the 2 cm luminosity of NGC 253 which is about hundred times less than their sample, the BBB luminosity for the nucleus is estimated to be $\sim 10^{42}$ ergs s^{-1} . This UV luminosity corresponds to an ionizing photon flux of $\sim 2 \times 10^{52} \text{ s}^{-1}$, consistent with the value derived from the observed RRLs. Based on the derived UV luminosity, the value of L_{2-10} was calculated for a range of input parameters (Frank, King and Raine 1985). It was found that the thin disk model under-predicts L_{2-10} , and is consistent with observations only for super-eddington accretion rates.

However, given the low radiative efficiency of the nucleus (the accretion rate is estimated to be less than 0.01 times the eddington rate), the AGN could be powered by an ADAF disk (Narayan, Mahadevan and Quataert 1998). ADAF models predict the absence of a BBB. The 2 cm radio luminosity of the nucleus of NGC 253 implies that the AGN is of low luminosity (LLAGN; Nagar et al. 2000) and these LLAGNs have been shown not to exhibit a BBB in their UV emission (Ho 1999). Hence we shall now try

² URL: <http://www.stsci.edu/science/starburst99/>

to explain the ionization from the X-ray luminosity instead. Pietsch et al. (2001) modeled the emission from the nuclear X-ray source as bremsstrahlung radiation from a three-temperature plasma. For simplicity, we shall assume that the UV up to X-ray emission is bremsstrahlung radiation from plasma at a single temperature, T_x . The UV portion of the emission is constrained to produce an ionizing photon flux greater than that needed to explain the RRLs and the 2–10 keV portion is normalized to the observed value. The required ionization is found to be consistent with the observed X-ray flux only for $T_x < 0.2$ keV. Since it is unlikely that most of the 2–10 keV emission arises in the exponentially decaying part of the thermal emission at 0.2 keV, this result is interpreted to imply that the X-ray emission is too weak to explain the required ionization.

8. DISCUSSION

8.1. *The star cluster model*

Given the uncertainty of stellar tracks, N_{Lyc} and L_{mech} predicted by the Starburst 99 code are not accurate to more than a factor of a few for $t < 5 \times 10^5$ years (Leitherer, private communication). The radius of the shock front is $R_s \sim (\int L_{\text{mech}} dt)^{1/5}$ in the energy-conserving phase. Since L_{mech} is a monotonically increasing function of time (up to 5×10^6 years for a continuous SFR), the dynamics of the nebula at $t > 5 \times 10^5$ years is insensitive to the uncertainties in the Starburst 99 model at earlier times. Hence we can conclude that a nebula older than this age will not be able to explain the observations. The only consistent nebular age estimate derived in section 6.1 is $\sim 2.5 \times 10^4$ years. The inputs from the Starburst 99 code are not accurate for such short timescales. Nevertheless it can be shown that since the ratio between L_{mech} and N_{Lyc} is constant with time, if just the functional dependence of L_{mech} with time for $t < 5 \times 10^5$ years is reliable, then the model results are relatively independent of the uncertainties in the Starburst 99 codes. However, given the short ages derived, it can be expected that the star formation at this timescale, and hence the value of L_{mech} and N_{Lyc} , is stochastic, in which case, the derived age is inconsistent with the assumptions in the model. Even for a stochastic star formation process, the short dynamical timescale of 10^4 years needs to be explained. The dynamical model implicitly assumes that the star cluster is spatially within the wind-blown structure, which need not be true for a ≤ 4 pc region. The model also assumes that the stellar wind of the individual stars add coherently to produce a total ‘cluster-wind’. This assumption will be violated for a young cluster due to stellar-wind collisions and YSO outflows. These factors may help confine the gas for a longer time and also provide a natural way of increasing the line width by stirring up the intra-cluster medium. Hence if a star cluster is invoked as an ionizing source, it must be fairly young, though the properties of such a young cluster cannot be easily predicted.

8.2. *The AGN model*

We have shown in section 7 that if the proposed AGN hosts a standard thin accretion disk with a BBB, then this disk produces enough UV radiation to ionize the RRL emitting gas but its X-ray emission falls short of the observed value. On the other hand, if the AGN has an ADAF

disk instead, then again, the observed X-ray emission is insufficient to ionize the RRL emitting gas. ADAF models also predict the X-ray emission for a given radio flux and mass of the black hole (Yi and Boughn 1998) and the estimated X-ray luminosity is a hundred times less than that observed (and is ten times less than the ratio observed in other LLAGNs; Ulvestad and Ho 2001). A possible way of explaining the observed radio and X-ray fluxes along with the required UV flux is the model of Quataert et al. (1999) who explain the spectrum of two LLAGNs which have an X-ray to UV ratio which is too large for a thin disk and too small for an ADAF disk. Following their work, we hypothesize that the possible AGN in the nucleus of NGC 253 has an ADAF disk in the interior, giving way to a standard thin disk beyond a certain radius. In this picture, the radio and the UV emissions arise in the outer disk (which would have a BBB in its spectrum) and the X-ray emission arises from the inner ADAF disk.

8.3. *The ionizing source*

It is clear from section 8.1 that if the ionizing source is a star cluster, its age must be at least younger than $\sim 10^5$ years. The AGN model, discussed in section 8.2, does manage to explain the observations but the constraints on this model are relatively less in number. The probability of detecting a star cluster of age $\lesssim 10^5$ years at the radio nucleus would be small. Since there is additional evidence supporting the existence of an AGN at the nucleus, we favor an AGN as the possible ionizing source. The existence of an AGN at the nucleus needs to be confirmed through high resolution radio continuum or X-ray imaging. The surrounding region has a transitional HII/weak-[O I] LINER spectrum (Engelbracht et al. 1998) and hence disentangling the optical signature of an AGN from this LINER emission will be difficult. Detailed multi-wavelength modeling of the nuclear emission also needs to be carried out in the framework of the AGN model in order to further constrain the properties of this object.

9. CONCLUSIONS

We have imaged the RRL emission from the starburst galaxy NGC 253 at 8.3 GHz and 15 GHz with a spatial resolution of $\sim 0.3''$ (~ 4 pc) using the VLA. The line emission is maximum at the radio nucleus at both frequencies and is much weaker near the position of the IR peak, which is known to host an SSC. The line widths of both RRLs are large: ~ 200 km s^{-1} . The continuum and line emission were modeled in terms of a uniform density photo-ionized gas. The observed RRLs can be explained as arising from a 2–4 pc sized region of gas of mass few thousand M_{\odot} , at a density of 10^4 cm^{-3} . The ionizing flux required is $6\text{--}20 \times 10^{51}$ photons s^{-1} . This gas can, in principle, be ionized by a compact SNR, a star cluster or by an AGN. The dust extinction against the nucleus is very high and hence direct detection of the ionizing source in the optical-IR is not feasible. Detailed dynamical modeling shows that a compact SNR cannot explain the observed properties of the ionized gas. The star cluster model was investigated in terms of a stellar wind-blown structure. Such a model can account for all of the observed properties only for a cluster

of age $\sim 2.5 \times 10^4$ years. Though this age estimate is shown not to be consistent with the dynamical model considered, a relatively young age ($\lesssim 10^5$ years) for any such cluster is unavoidable. If an AGN is assumed to be the ionizing source, then the observed X-ray flux cannot explain the required ionizing photon rate. However, a simple thin accretion disk model can account for the ionization based on the observed radio flux density. A composite model involving an inner thin disk and an outer ADAF disk is suggested, in order to simultaneously explain the radio, UV and the X-ray observations.

The detection of such a young star cluster at the nucleus of the galaxy is improbable. Since there is additional evidence supporting the existence of an AGN at the nucleus from radio continuum data, we favor the AGN model as an ionizing source. If confirmed, our observations could be the first detection of RRLs from an AGN outside our galaxy. The central ~ 36 pc region of NGC 253 is host to a number of compact thermal and non-thermal sources and

diffuse gas and is also coincident with the base of the galactic superwind and possibly hosts a central AGN as well. Hence this galaxy would be an ideal laboratory to study the dynamics and the interaction of all these components, much like the galactic center.

The National Radio Astronomy Observatory is a facility of the National Science Foundation operated under cooperative agreement by Associated Universities, Inc. This research has made use of the Starburst 99 code, made available to the public by the authors and we thank them for sharing it with the community. This research has made use of NASA's Astrophysics Data System Abstract Service. We thank Dipankar Bhattacharya, K. S. Dwarakanath, Kelsey Johnson, Biman Nath, Prasad Subramanian and Jim Ulvestad for detailed discussions and helpful comments. We also wish to thank the referee for many insightful comments which helped in improving the clarity of the paper.

REFERENCES

- Anantharamaiah, K. R., Zhao, J. -H., Goss, W. M., & Viallefond, F. 1993, *ApJ*, 419, 585
- Anantharamaiah, K. R. & Goss, W. M. 1996, *ApJ*, 466, L13
- Antonucci, R. R. J. & Ulvestad, J. S. 1988, *ApJ*, 330, L97
- Beck, S. C., & Beckwith, S. V. 1984, *MNRAS*, 207, 671
- Böker, T., Krabbe, A., & Storey, J. W. V. 1998, *ApJ*, 498, L115
- Chevalier, R. A. & Fransson, C. 2001, *ApJ*, 558, L27
- Draine, B. T. & Woods, D. T. 1991, *ApJ*, 383, 621
- Engelbracht, C. W., Rieke, M. J., Rieke, G. H., Kelly, D. M., & Achtermann, J. M. 1998, *ApJ*, 505, 639
- Falcke, H., Malkan, M. A., & Biermann, P. L. 1995, *A&A*, 298, 375
- Forbes, D. A., Ward, M. J., Depoy, D. L. 1991, *ApJ*, 380, L63
- Forbes, D. A., Ward, M. J., Rotaciuc, V., Blietz, M., Genzel, R., Drapatz, S., van der Werf, P. P., Krabbe, A. 1993, *ApJ*, 406, L11
- Forbes, D. A., Polehampton, E., Stevens, I. R., Brodie, J. P., & Ward, M. J. 2000, *MNRAS*, 312, 689
- Frank, J., King, A. R., & Raine, D. J. 1985, *Accretion power in astrophysics* (Cambridge University Press)
- Ho, L. C. 1999, *ApJ*, 516, 672
- Huang, Z. P., Thuan, T. X., Chevalier, R. A., Condon, J. J., & Yin, Q. F. 1994, *ApJ*, 424, 114
- Kalas, P., & Wynn-Williams, C. G. 1994, *ApJ*, 434, 546
- Keto, E., Ball, R., Arens, J., Jernigan, G., Meixner, M., Skinner, C., & Graham, J. 1993, *ApJ*, 413, L23
- Keto, E., Hora, J. L., Fazio, G. G., Hoffmann, W., & Deutsch, L. 1999, *ApJ*, 518, 183
- Kobulnicky, H. A., & Johnson, K. E. 1999, *ApJ*, 527, 154
- Koratkar, A. & Blaes, O. 1999, *PASP*, 111, 1
- Leitherer, C., et al. 1999, *ApJS*, 123, 3
- McCray, R. 1983, in *Highlights of Astronomy*, Vol. 6, ed. R. West (Dordrecht: Reidel), 565
- Mebold, U., Shaver, P. A., Bell, M. B., & Seaquist, E. R. 1980, *A&A*, 82, 272
- Meurer, G. R., Heckman, T. M., Leitherer, C., Kinney, A., Robert, C., & Garnett, D. R. 1995, *AJ*, 110, 2665
- Mohan, N. R., Anantharamaiah, K. R., & Goss, W. M. 2001, *ApJ*, 557, 659
- Muñoz-Tuñón, C., Tenorio-Tagle, G., & Castañeda, H. O. 1996, *AJ*, 112, 1636
- Nagar, N. M., Falcke, H., Wilson, A. S., & Ho, L. C. 2000, *ApJ*, 542, 186
- Narayan, R., Mahadevan, R., & Quataert, E. 1998, in *Theory of Black Hole Accretion Disks*, ed. M. A. Abramowicz et al. (Cambridge University Press), 148
- Neff, S. G., & Ulvestad, J. S. 2000, *AJ*, 120, 670
- Newman, W. 1977, *Ap&SS*, 47, 99
- Pietsch, W. et al. 2001, *A&A*, 365, L174
- Piña, R. K., Jones, B., Puetter, R. C., & Stein, W. A. 1992, *ApJ*, 401, L75
- Puxley, P. J., Mountain, C. M., Brand, P. W. J. L., Moore, T. J. T., Nakai, N. 1997, *ApJ*, 485, 143
- Quataert, E., Di Matteo, T., Narayan, R., & Ho, L. C. 1999, *ApJ*, 525, L89
- Sams, B. J. III, Genzel, R., Eckart, A., Tacconi-Garman, L., & Hofmann, R. 1994, *ApJ*, 430, L33
- Shull, J. M. 1980, *ApJ*, 238, 860
- Spitzer, L. 1968, *Diffuse Matter in Space* (New York: Interscience)
- Tarchi, A., Neininger, N., Greve, A., Klein, U., Garrington, S. T., Muxlow, T. W. B., Pedlar, A., & Glendenning, B. E. 2000, *A&A*, 358, 95
- Turner, J. L., Beck, S. C., & Ho, P. T. P. 2000, *ApJ*, 532, L109
- Turner, J. L., & Ho, P. T. P. 1985, *ApJ*, 299, L77
- Ulvestad, J. S., & Antonucci, R. R. J. 1997, *ApJ*, 488, 621
- Ulvestad, J. S. & Ho, L. C. 2001, *ApJ*, 562, 133
- Vacca, W. D., Garmany, C. D., & Shull, J. M. 1996, *ApJ*, 460, 914
- Watson, A. M., et al. 1996, *AJ*, 112, 534
- Yi, I. & Boughn, S. P. 1998, *ApJ*, 499, 198
- Yorke, H. W., Tenorio-Tagle, G., & Bodenheimer, P. 1984, *A&A*, 138, 325

TABLE 1
VLA observational log and image parameters

Parameter	8.3 GHz data	15 GHz data
Date of observation	9/7/99, 12/7/99 & 9/10/99	26/6/99
ν_{rest} of RRL (GHz)	8309.4 (H92 α)	15281.5 (H75 α)
Bandwidth (MHz), channels/IF	24.2, 31	46.9, 15
Spectral resolution ^a (km s ⁻¹)	56.4	122.6
Shortest baseline (k λ)	7	12
Beam (natural weights)	0.5'' \times 0.28''	0.31'' \times 0.14''
Phase calibrator	0116-219	0118-272
Bandpass calibrator	2251+158	2251+158
Peak continuum flux density ^b (mJy)	40	37
Peak line flux density (mJy)	0.92 \pm 0.02	1.72 \pm 0.02
Noise in the continuum image (1 σ , mJy)	0.04	0.13
Line strength ^c ($\times 10^{-23}$ W/m ²)	6 \pm 1	23 \pm 2
FWHM of line ^d (km s ⁻¹)	225 \pm 15	197 \pm 26
Noise per channel (mJy)	0.14	0.35

^aThe spectral resolution after off-line hanning smoothing.

^bEvaluated by simultaneously fitting a gaussian, a zero level and a slope.

^cCorresponding to the spectrum against the unresolved radio nucleus.

^dThe FWHM after deconvolving the effects of hanning smoothing and finite spectral resolution.

TABLE 2
RRL model details (spherical geometry)

Parameter	Range
<i>Explored input parameter space</i>	
Electron temperature (T_e , K)	2500–12500
Local electron density (n_e , cm ⁻³)	10 ⁻² –10 ⁶
Diameter (l , pc)	0.01–5.0
<i>Model solutions for $T_e=5000-12500$ K</i>	
n_e (cm ⁻³)	6000–17000
l (pc)	2–5.0
N_{Lyc} (s ⁻¹)	(6–20) \times 10 ⁵¹
M_{HII} (M_{\odot})	1000–7000
Stimulated emission (at 15 GHz, %)	10–60
Thermal continuum fraction (15 GHz)	0.15–0.7

TABLE 3
Typical model results : for a spherical geometry with $T_e=7500$ K.

Parameter	$n_e=7000 \text{ cm}^{-3}$			$n_e=17000 \text{ cm}^{-3}$		
	A ^a	B	C	A	B	C
Diameter l (pc)	3.1	4.0	3.5	2.1	2.3	2.1
$N_{\text{Lyc}} (\times 10^{52} \text{ s}^{-1})$	0.8	1.6	1.0	1.4	1.9	1.4
$S_{\text{th}}/S_{\text{total}}$ at 15 GHz	0.3	0.6	0.4	0.4	0.5	0.4
Stimulated emission ^b (%)	55	0	—	22	0	—
Spectral index ^c ($S_\nu \propto \nu^{-\alpha}$)	0.45	0.5	0.45	0.7	0.75	0.7
$M_{\text{HII}} (M_\odot)$	2800	6000	3700	2100	2800	2200

^aA, B, and C refer to models where the unabsorbed continuum radiation is assumed to be behind, in front of, and mixed with, the ionized gas.

^bThe fraction of H75 α line emission due to stimulated emission by the background radiation.

^cAverage spectral index of the unabsorbed continuum radiation, excluding the thermal contribution of the ionized gas.

TABLE 4
Dynamical modeling details

Parameter	Explored Range	Solutions obtained
<i>Parameter space for model inputs</i>		
Ambient density (n_0, cm^{-3})	10^{-3} – 10^6	200–400
Age of cluster (yrs)	10^4 – 10^8	$(2\text{--}3.5) \times 10^4$
SFR (M_\odot/yr)	0.1–100.0	2.5–6
<i>Parameter space for observational constraints</i>		
Radius of shell (R_s, pc)	0.2–4.0	3.5–4.0
Velocity of shell ($V_s, \text{km s}^{-1}$)	80–120	85–115
Mass of ionized gas (M_\odot)	1250–5000	1250–2400
N_{Lyc} (photons s^{-1})	$6\text{--}24 \times 10^{51}$	$6\text{--}10 \times 10^{51}$
Density of ionized gas (n_e, cm^{-3})	$(4\text{--}25) \times 10^3$	$(18\text{--}25) \times 10^3$

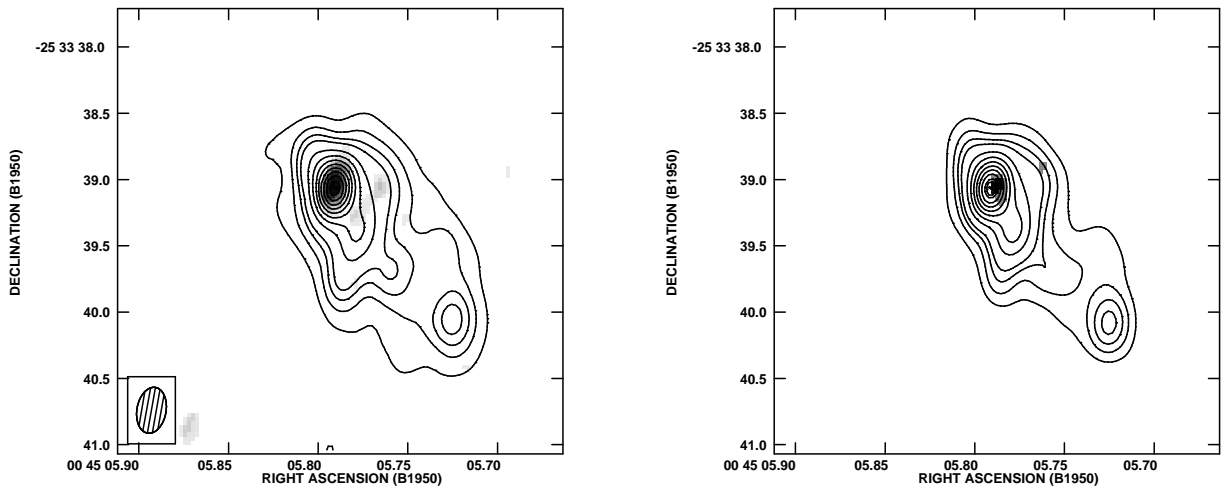


FIG. 1.— The radio continuum emission at 8.3 GHz (*left*) and 15 GHz (*right*) of the central 36 pc of NGC 253 are plotted as contours. The contour levels in mJy are 4, 6, 8, 10 and then higher in steps of 5 mJy. The line emission integrated over the velocity range $100\text{--}400 \text{ km s}^{-1}$ for the H92 α and H75 α RRLs are overlaid in greyscale. The beam size for both the images is $0.35'' \times 0.22''$ at a P.A. of -10° and is shown at the bottom left corner of the left-hand side image.

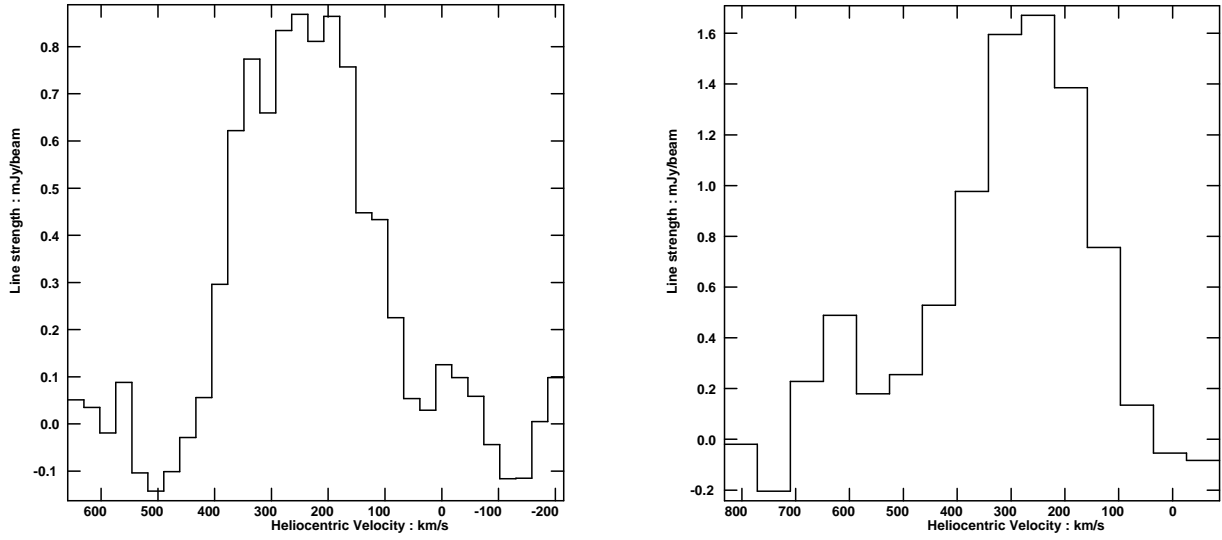


FIG. 2.— Hanning smoothed spectra of H92 α RRL at 8.3 GHz (*left*) and H75 α RRL at 15 GHz (*right*) against the radio nucleus, for a resolution element of $0.35'' \times 0.22''$. The velocity resolution is 56.4 km s^{-1} and 122.6 km s^{-1} for the H92 α and H75 α spectra respectively.